Polymer Chemistry

Accepted Manuscript

ROYAL SOCIETY OF CHEMISTRY

www.rsc.org/polymers

Cite this: DOI: 10.1039/c0xx00000x

www.rsc.org/xxxxxx

Paper

One-Pot Synthesis of Highly Cross-linked Fluorescent Polyphosphazene nanoparticles for Cell Imaging

Lingjie Meng*[a], Chengqiang Xu[b], Tianhui Liu[a], Hua Li[c], Qinghua Lu*[b], and Jiangang Long[c]

Received (in XXX, XXX) Xth XXXXXXXXX 20XX, Accepted Xth XXXXXXXXX 20XX

DOI: 10.1039/b000000x

Highly cross-linked and monodisperse polyphosphazene nanoparticles (NPs) exhibiting strong fluorescence were prepared by a remarkably simple one-pot polycondensation of hexachlorocyclotriphosphazene (HCCP) and 4,5-dibromofluorescein (DBF). The morphology and size of the resulting poly(cyclotriphosphazene-co-dibromofluorescein) (PCTPDBF) NPs can be facilely tuned by varying the solvent and reactant concentration. The fluorescent DBF units were isolated and "fastened" in the cross-linked structures, which can well suppress the concentration-quenching effect of small fluorescent probes. Hence, the PCTPDBF NPs emitted bright yellow fluorescence at any concentration. The PCTPDBF NPs could enter HeLa and H9C2 cells and were located in the cytoplasm. Combined with their excellent biocompatibility and improved resistance to photobleaching and protein interference, they can be used as ideal fluorescent agents for cell imaging.

1. Introduction

Fluorescence bio-imaging techniques have attracted tremendous interests because they provide powerful tools for investigating several fundamental life and biomedical processes[1, 2]. Various fluorescence-based assays have been used for the real-time observation of organs, cells, and even biomolecules with 3D landscape models or nanometer spatial resolution; thus, a broad range of biological activities can be monitored, and structure–activity relationships of biomolecules can be investigated[3-5]. Exogenous fluorophores with a suitable wavelength, strong brightness, good biocompatibility, and high resistance to photobleaching and protein interference are often needed to be used for a fluorescence technique to provide high quality and reliable imaging.

Typically, bioimaging fluorophores such as fluorescent proteins[6, 7], semiconductor quantum dots (QDs)[8, 9], rare-earth-based NPs[10, 11], carbon dots[12, 13], organic dyes, and dye-doped NPs[14-16] have been used. Fluorescent proteins represent a type of considerable toolkit with excellent biocompatibility and biospecificity. They have been widely used for studying gene expression, protein transport, and other cellular processes. However, only a small selection of fluorescent proteins is available; in addition, they generally exhibit poor resistance to photobleaching.[17] Furthermore, it is difficult to synthesize red and near-infrared fluorescent proteins for whole-body fluorescence imaging. QDs and rare-earth-doped NPs exhibit broad absorption bands, tunable emissions with sharp and symmetric peaks, high brightness, and excellent photostability, making them attractive contrast agents in biomedical imaging. The major lingering problem of QDs and rare-earth-doped NPs is their inherent cytotoxicity, because the heavy metal constituents of QDs and rare earth NPs such as cadmium, selenium, and neodymium are highly toxic to many cells and tissues, especially when the hydrophilic shell around the NPs is not stable[18, 19]. Carbon dots is an emerging class of fluorescent carbon nanomaterials with some unique properties such as tunable luminescence, superior chemical and fluorescence stability, excellent biocompatibility, and versatile surface chemistry. Most carbon dots emitted strong blue or green flurescence under irradiation of UV light, a major challenge is the synthesis of carbon dots with brighter fluorescence emissions excitable by red or NIR sources.[20, 21] Organic dyes such as fluorescein, rhodamine, and cyanine appear to be the most versatile fluorophores used in biological imaging and bioassays. The optical properties of dye molecules can be fine-tuned by various design and synthetic strategies. However, intrinsic limitations of conventional dyes such as the concentration-quenching effect[22] and poor photostability[23] have posed considerable difficulties for the further development of high-sensitivity imaging techniques and high-throughput assays. As a result, dye-doped silica or polymer NPs represents the most abundant structural fluorescent NPs for bioimaging. They usually incorporate dye molecules inside a silica or polymer particle by covalent attachment or physical entrapment and exhibit higher brightness and better photostability than molecular dyes because of the large number of fluorophores per particle and the protective matrix.[24] However, in practice, organic dyes tend to aggregate together and lead to fluorescence quenching or leak from the NPs.[25] Hence, it is an ongoing challenge to design and synthesize brightly fluorescent NPs with tunable emissions, high chemical and optical stability, good water dispersibility, and biocompatibility for fluorescence bioimaging techniques.

Tang et al proposed an aggregation-induced emission (AIE)

mechanism in 2001, the non-planar molecules might effectively overcome the aggregation-caused quenching by the restriction of the intramolecular rotation.[22, 26] Recently, we developed another new strategy to "isolate" and "fasten" fluorescent moieties such as porphyrins into stable cross-linked polyphosphazene (PZS)[27]. Thus, each fluorescent moiety can exhibit improved resistance to photobleaching and isolated single-molecule performance (*i.e.,* high fluorescence efficiency) at any concentration. This universal strategy opened a door to fix other dyes into the cross-linked structures for various applications. Because of the excellent biocompatibility of the PZS skeleton, this study reports the first example of fastening a non-toxic dye such as 4,5-dibromofluorescein (DBF) into cross-linked PZS NPs for bioimaging. The effect of solvent and reactant concentration on the morphology and size of poly(cyclotriphosphazene-co-dibromofluorescein) (PCTPDBF) NPs was systematically investigated. Since cyclotriphosphazene moieties may serve as spacers to effectively overcome the concentration-quenching effect of DBF, the resulting PCTPDBF NPs emitted strong yellow fluorescence. Interestingly, the PCTPDBF NPs inherit outstanding thermal stability, solvent resistance, water dispersion, and biocompatibility of PZS,[28, 29] and exhibit some new improved fluorescence properties as compared to DBF, such as excellent resistance to photobleaching and protein interference. Therefore, the fluorescent NPs were studies for their potential applications in cell imaging.

2. Experimental Section

2.1 Chemicals:

DBF (95%) and hexachlorocyclotriphosphazene (HCCP, 98%) were purchased from Aladdin Reagent Corporation. Trimethylamine and bovine serum albumin (BSA) were obtained from Shanghai Chemical Reagent Corporation. Fetal bovine serum (FBS) and high-glucose Dulbecco's modified Eagle's medium (DMEM) were obtained from Hyclone. 3-(4,5-dimethyl-2-thiazolyl)-2,5-diphenyl-2-H-tetrazolium bromide (MTT) reagent was purchased from Beyondtime Bio-Tech, China. 4′,6-Diamidino-2-phenylindole dihydrochloride (DAPI, 98%) was purchased from Sigma. All other organic solvents such as acetonitrile, acetone, and anhydrous ethanol were of analytical grade and were used as received. Water was purified using a Milli-Q-system (Millipore, Bedford).

2.2 Preparation of PCTPDBF NPs

In a typical procedure, HCCP (15 mg, 43.1 μmol), DBF (32 mg, 65.3μmol), and acetonitrile (50 mL) were added into a 100 mL round-bottom flask. After ultrasonic irradiation for 20 min (50 W, 40 kHz), 2 mL of triethylamine was added. The solution was then maintained at room temperature for 3 h under ultrasonic irradiation (50 W, 40 kHz). As soon as the reaction was completed, the resulting products were collected by centrifugation, successively washed with anhydrous alcohol (3×30 mL) and deionized water (3×30 mL), and dried at 45 °C under vacuum overnight. Yield 44 %. To investigate the effect of the solvent and reactant concentration on the morphology and size of PCTPDBF NPs, the solvent was changed to acetone or a mixture of acetone/acetonitrile (v/v= 8:2, 5:5, or 2:8), and the reactant concentration was changed to double and half, respectively. Each reaction condition was conducted in duplicate.

2.3 Cell Viability Test

The MTT assay was used to measure cell viability.[30, 31] In brief, human cervical carcinoma HeLa cells and human H9C2 cells were seeded into 24-well flat culture plates (Corning) and cultured in DMEM supplemented with 10% FBS at 37°C in a humidified incubator (MCO-15AC, Sanyo) in which the CO_2 level was maintained constant at 5%. After culturing overnight, the cells were washed with FBS-free DMEM and incubated with a specific concentration of PCTPDBF NPs (10, 25, 50, and 100 μg/mL) in a FBS-free culture medium at 37 °C for 24 and 48 h. The cells were then washed with PBS, and FBS-free DMEM (180 μL) was used to substitute the culture medium before adding 20 μL of MTT reagent (5 mg/mL). After incubation for 4 h at 37 °C, the media was removed, and 150 μL DMSO was added to each well and pipetted up and down to dissolve crystals. The absorbance was then measured at 570 nm using a microplate reader (Model 680, Bio-Rad). Background absorbance was measured at 570 nm before adding the MTT reagent, and the cells cultured in the absence of PCTPDBF NPs were used as controls.

2.4 Cell Imaging by Confocal Laser Scanning Microscopy

To investigate the cell-imaging capacity of the PCTPDBF NPs, confocal laser scanning microscopy was employed. Human cervical carcinoma HeLa cells and human H9C2 cells were seeded into a 24-well flat culture plate (Corning) and cultured in DMEM supplemented with 10% FBS at 37°C overnight. The cells were washed with FBS-free DMEM and incubated with PCTPDBF NPs (50 μg/mL) in a FBS-free culture medium at 37 °C for 2h. The cells were then washed with PBS and FBS-free DMEM to remove the free PCTPDBF NPs from the culture medium. The cells were then observed under a confocal laser scanning microscope.

2.5 Characterization

Transmission electron microscopy (TEM) was carried out on a CM120 (Philips). The elemental composition of samples was determined by energy dispersive spectrometer (EDS, Link-Inca 622, U.K.) on the TEM. Field emission scanning electron microscope (FESEM) images were obtained using a Philips Sirion 200 instrument under an accelerating voltage of 20 kV. The size and distribution of all as-prepared nanomaterials were determined from TEM and SEM micrographs using ImageJ (V1.41, NIH, USA) for image analysis. Photographs were taken with a digital camera (IXUS 800IS, Canon, Japan). Fourier-transform infrared (FTIR) spectra were recorded on a Paragon 1000 (Perkin Elmer) spectrometer. Samples were dried overnight at 45 ºC under vacuum and thoroughly mixed and crushed with KBr to fabricate KBr pellets. X-ray photoelectron spectroscopy (XPS) experiments were carried out on a RBD upgraded PHI-5000C ESCA system (Perkin Elmer) with Mg Ka radiation (hv = 1253.6 eV) or Al Ka radiation (hv = 1486.6 eV). Ultraviolet and visible (UV-Vis) absorption spectra were recorded on an Shimadzu UV-2550 spectrophotometer. The fluorescence spectra were performed on a Perkin–Elmer LS 50B fluorescence spectrometer. The fluorescence quantum yields were measured by a FLS920 lifetime and steady state spectrometer with a calibrated integrating sphere (Edinburgh). Thermogravimetric analysis

(TGA) curves (heating rate = 10 ºC·min^{-1} in nitrogen) were recorded on TGA-7 (Perkin Elmer) instruments. Fluorescence images of cells were taken on a LSM700 confocal laser scanning microscopy (Carl Zeiss).

3. Results and Discussion

The fluorescent PCTPDBF NPs were prepared by a very simple one-pot polycondensation of HCCP and DBF (**Scheme 1**). First, TEA activated the phenolic hydroxyl groups of DBF, followed by the attack of the nucleus of the phosphorus atom in HCCP to generate a pre-polymer and HCl under ultrasonication. Excess TEA as an acid acceptor can further absorb the resulting HCl and accelerate polymerization. Although only one chlorine atom at most can be replaced by DBF on each phosphorus atom because of steric hindrance, the resulting PCTPDBF NPs should have a highly cross-linked structure. As polymerization proceeds, the grown monodisperse PCTPDBF NPs gradually precipitated from the solvent. Solvent polarity remarkably affected the reaction rate. For example, PCTPDBF NPs rapidly formed and precipitated in acetonitrile within several minutes, whereas precipitates formed rather slowly in acetone, *i.e.,* several hours.

The size and morphology of the as-synthesized PCTPDBF NPs were investigated by transmission electron microscopy (TEM) and field-emission scanning electron microscopy (FESEM). Typically, PCTPDBF NPs obtained by the reaction of HCCP (15 mg) and DBF (32 mg) in acetonitrile were monodisperse nanospheres with a relatively smooth surface (**Figure 1a** and **b**), and their average diameter was approximately 322.6 ± 8.0 nm (**Figure 1d**). The central portion of each particle was darker than its edge, indicative of solid nanospheres. As observed in FESEM images, the NPs were approximately 354.0 nm nanospheres (**Figure 1c**), which is in good agreement with that of TEM images.

Interestingly, the size of PCTPDBF NPs can be facilely adjusted by tuning the initial reactant concentration. In all experiments, we fixed the amount of acetonitrile and triethylamine at 50 mL and 2 mL, respectively, and adjusted the DBF and HCCP concentrations. Compared to the size of the PCTPDBF NPs in Figure 1, that of NPs decreased to approximately 200 nm (**Figure 2a-c**) at DBF and HCCP concentrations of 7.5mg and 16 mg, respectively. Since the reaction rate of precipitation polymerization in acetonitrile is rapid, the reactants may be exhausted because of their relatively low concentration before the NP size increased. Moreover, when the DBF and HCCP concentrations were increased to 30 mg and 64 mg, larger NPs of approximately 400 nm were obtained (**Figure 2d–f**).

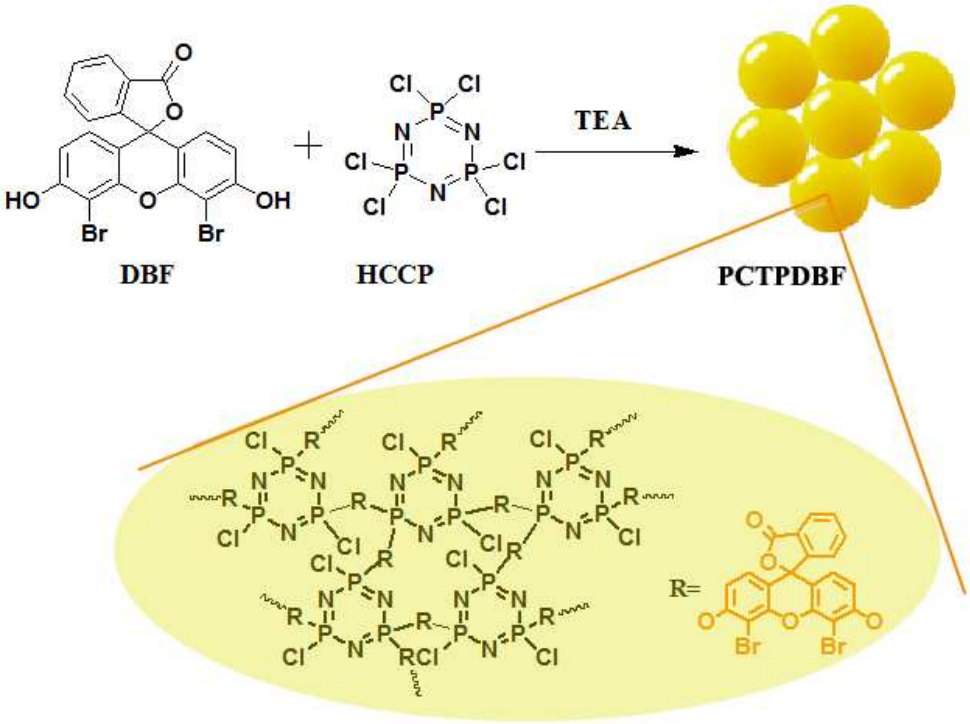

Scheme 1 Synthetic route to fluorescent PCTPDBF NPs.

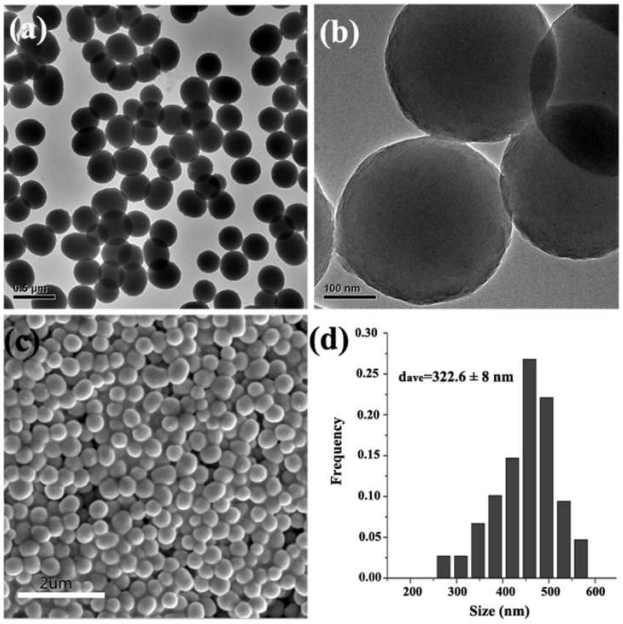

Fig. 1 (a, b) TEM images and (c) SEM image of PCTPDBF NPs obtained in acetonitrile, (d) size distribution graph of the NPs in (a)..

The effect of the solvent on precipitation polymerization was also investigated. Solvents not only affect the reaction rate but also play a key role in the size and morphology of the resulting PCTPDBF NPs because different organic solutions have different polarity and Hildebrand solubility parameters.[32] Different from the isolated and monodisperse nanospheres obtained in acetonitrile, only some irregular particles blended and fused with each other were observed in acetone (see Supporting Information, **Figure S1**). The reaction rate was relatively low in acetone due to the weak polarity of acetone. In addition, both DBF and PCTPDBF exhibited better solubility in acetone than in acetonitrile, leading to irregular and adhesive particles. To systematically study the influence of solvent on the morphology of products, mixed solvents composed of a different ratio of acetone/acetonitrile were used (see Supporting Information, **Figure S2**).We maintained the amounts of DBF and HCCP at 7.5 and 16 mg, respectively, and changed the volume ratio of acetone to acetonitrile at 8:2, 5:5, or 2:8. With the increase of acetonitrile concentration, irregular and fused particles gradually decreased. Isolated and monodisperse nanospheres can be well prepared when the volume ratio of acetone to acetonitrile was 2:8. These results indicate that the reaction rate and morphology of PCTPDBF NPs can be well tuned by using an appropriate solvent.

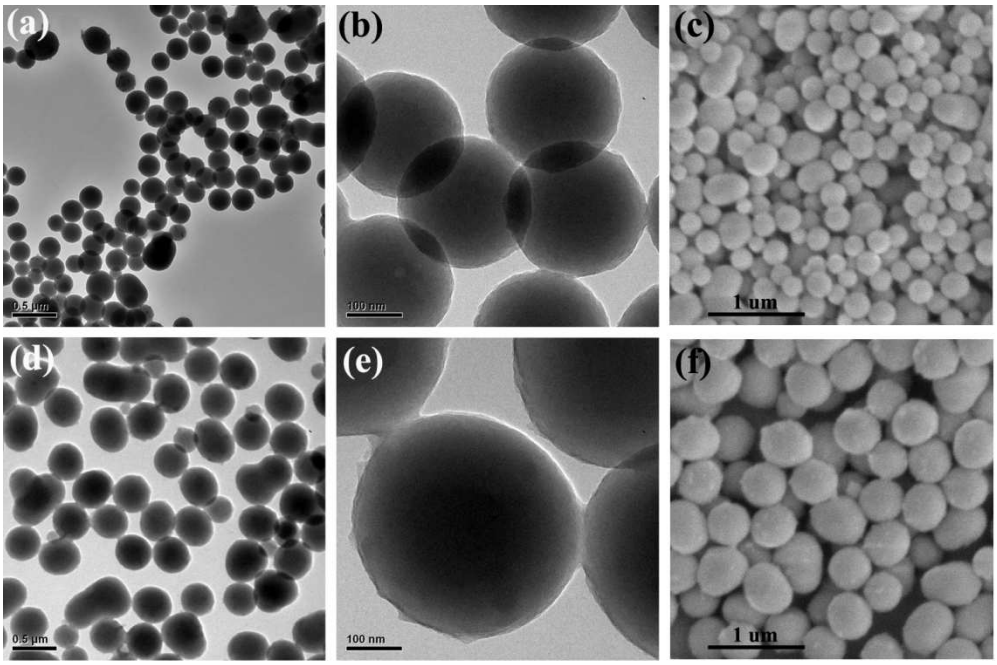

Fig. 2 TEM and SEM images of PCTPDBF NPs obtained in acetonitrile by reaction of (a–c) 7.5 mg HCCP and 16 mg DBF, (d–f)30 mg HCCP and 64 mg DBF.

FTIR spectroscopy was used to confirm the successful formation of PCTPDBF (Figure3a). Absorption peaks at 626 and 530 cm^{-1} attributed to P–Cl weakened in the DBF-PZS spectrum compared to that of HCCP, while a new intensive absorption peak at 943 cm^{-1}assigned to P–O–Ph band appeared, which are direct evidence of the polymerization of HCCP and DBF[33, 34]. Other characteristic peaks of PCTPDBF can also be observed, including 1184 cm^{-1} (P=N), 882 cm^{-1} (P−N) in the cyclotriphosphazene structure, and 1773 cm^{-1} (carboxylic ester),1588 cm^{-1} and 1502 cm^{-1} (phenyl), and 1105 cm^{-1} and 1050 cm^{-1} (C−O−C) in the DBF units.

The elemental composition of PCTPDBF particles was determined by energy-dispersive spectroscopy (EDS, see Supporting Information, **Figure S3**) and X-ray photoelectron spectroscopy (XPS, Figure 4). Signals for C, N, O, P, Cl, and Br were all observed in the EDS spectrum, indicating that the chlorine atoms were not completely replaced. The signal of Cu possibly originates from the copper grid. XPS further provides

quantitative information that the molar ratio of phosphorus (2p, 133.1 eV) to chloride (2p3, 199.0 eV) is approximately1:1.04. It suggests that only one chlorine atom might be replaced by DBF on each phosphorus atom due to the steric hindrance effect. And yet for all that, a highly cross-linked structure should be obtained as shown in Scheme 1, and PCTPDBF particles hence exhibit excellent thermal stability. The onset of the thermal degradation temperature (T_d) of PCTPDBF was around 332 °C, and it exhibited a weight loss of only 34% under nitrogen at 600 °C (Figure 3b). In addition, the molar ratio of phosphorus (2p, 133.1 eV) to nitrogen (1s, 396.4 eV) was 1:0.97, which was in agreement with the theoretical results. The percentage of Br atoms (3d, 69.1 eV) was approximately two times that of P and N atoms, suggesting that the PCTPDBF particle surface is richer with DBF moieties than cyclotriphosphazene moieties.

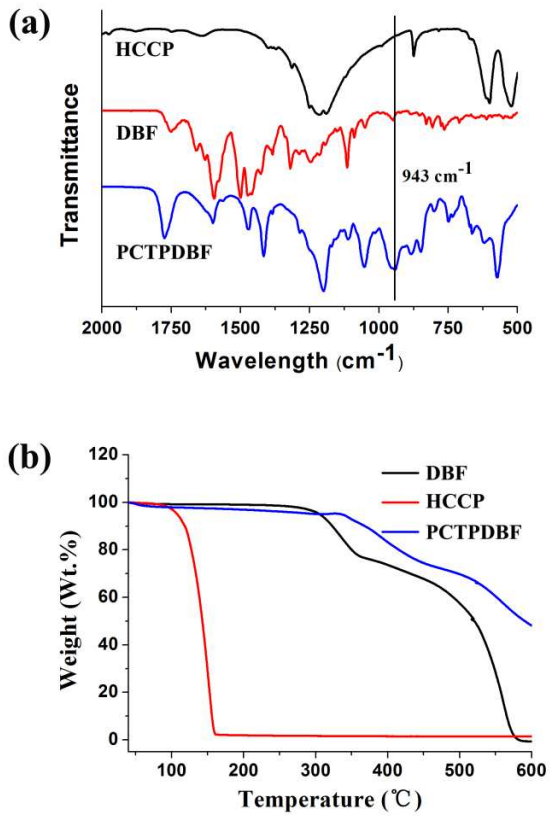

Fig. 3 (a) FTIR spectra and (b) TGA curves of DBF, HCCP, and PCTPDBF NPs.

The optical absorption and photoluminescence properties of DBF and PCTPDBF solutions were compared. Because of the presence of electronegative N, P, and S atoms, and especially active phenolic hydroxyl groups on the surface, PCTPDBF NPs were well dispersed in water and other polar solvents. The BDF ethanol solution exhibited a sharp absorption peak at around 535 nm with yellow color (Figure 5a). While the PCTPDBF dispersion in ethanol exhibited a red-shifting peak at 550 nm and a broad peak between 450 and 500 nm, which are attributed to the characterization peak of DBF moieties and the scattering of NPs, respectively. The PCTPDBF ethanol dispersion exhibited a pink color due to their strong extinction property between 400 and 570 nm. The DBF and PCTPDBF NPs exhibited strong emission peaks at approximately 530 and 560 nm under irradiation of 365nm light, respectively (Figure 5b). Thus, DBF exhibits yellowish-green fluorescence, while PCTPDBF NPs exhibit yellow fluorescence (see the inset in Figure 5b). The absorption and photoluminescence peaks of DBF moieties in PCTPDBF NPs are red-shifted probably because the connected hexahydroxy N,P-heterocycle changed the energy gap for the electron transition of DBF moieties in the NPs. The PCTPDBF NPs prepared in both acetone and acetonitrile exhibited the same fluorescence property (see Supporting Information, **Figure S4**), indicating that DBF moieties have the same chemical and physical state in these NPs.

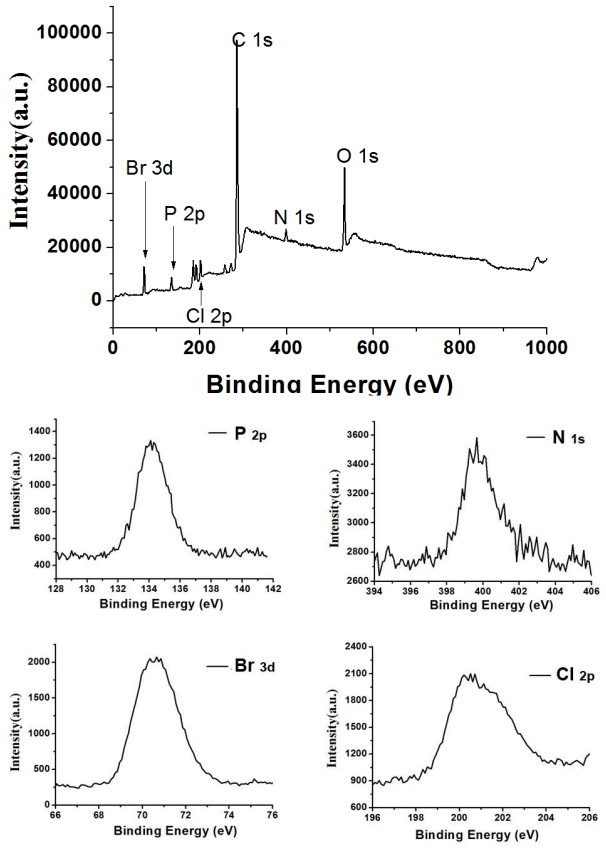

Fig. 4 XPS spectrum of PCTPDBF NPs, and high-resolution P 2p, N 1s, Br 3d, and Cl 2p XPS spectra.

The quantum yields (QY) of PCTPDBF NPs in ethanol and water (pH = 7) were 2.9 % and 1.6 %, respectively, which is lower than that of DBF in ethanol (16.7 %) and water (8.1%, pH=7). The major possible reasons were that only the DBF moieties near the surface of NPs could be irradiated and the scattering of NPs further reduced the QY. However, the PCTPDBF NPs could overcome effectively the aggregation-caused quenching of DBF moieties. The PCTPDBF powder emitted strong orange luminescence under irradiation of 365 nm light (see Supporting Information, **Figure S5**). Whereas DBF powder completely lost its fluorescence because DBF molecules have conjugate structures and tend to aggregate at high concentration by π-π stacking, leading to fluorescence quenching. It has been reported that cyclotriphosphazene rings are non-conjugated systems and are photochemically inert,[35] although their backbone formally consists of alternating single and double

P–N bonds. Therefore, cyclotriphosphazene rings serve as spacers to isolate the DBF moieties for preventing the transfer of the excited electrons in DBF moieties, thereby reducing fluorescence quenching.

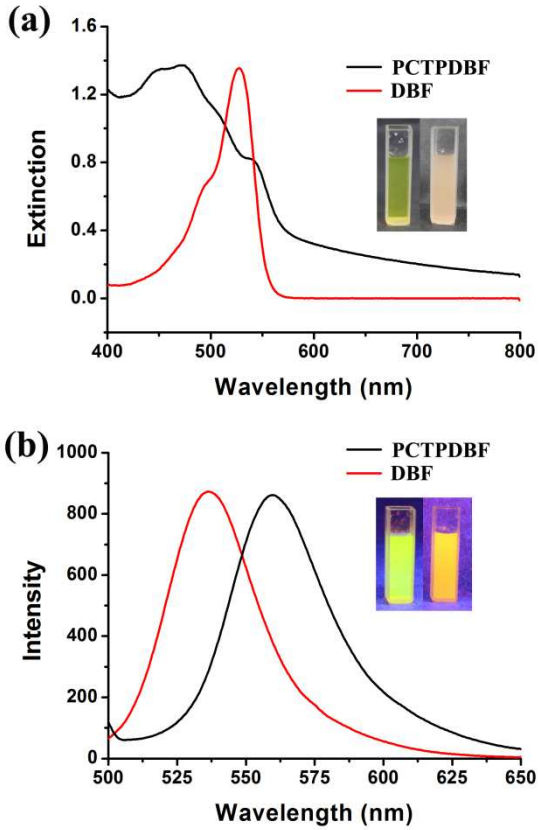

Fig. 5 (a) UV–Vis spectra and (b) Fluorescence spectra of DBF (50 ug/mL) and PCTPDBF NPs (300 ug/mL) in ethanol. The inset photographs are ethanol solutions of BDF (left) and PCTPDBF (right) under (a) natural light and (b) 365nm UV light.

Photostability is a particularly important criterion as it is often desirable to observe markers for extended periods of time against the background of intrinsic cellular emissions.[24, 36] Similar to many other fluorescent dyes, DBF exhibited clear photobleaching properties. Its fluorescence intensity rapidly decreased with the elongation of irradiation time in the experiment of continuously repeated excitations (Figure 6a). Remarkably, the PCTPDBF NPs were quite stable with respect to irradiation, exhibiting a negligible reduction in the observed intensities for 130 min (Figure 6b). For comparison, Figure 6c also shows the bleaching behavior of DBF and PCTPDBF NPs. The PCTPDBF NPs exhibited superior resistance to photobleaching, indicating that the DBF moieties have improved photochemical stability after being "fastened" in the cross-linked structures.

The fluorescence of materials might also be affected by biomolecules, except photobleaching in complex biological environments[37-39]. The fluorescence intensity of DBF markedly decreased when it was mixed in BSA solution and stirred for 2 h due to the interactions between DBF and BSA. With the increase of the BSA concentration, the fluorescence of DBF was weaker (Figure 7a), whereas the fluorescence of PCTPDBF was highly stable with just slight fluorescence quenching(Figure 7b), because most of the DBF moieties are fixed in the NPs and cannot interact with BSA. The improved resistance of PCTPDBF NPs to protein interference benefits their bioimaging applications.

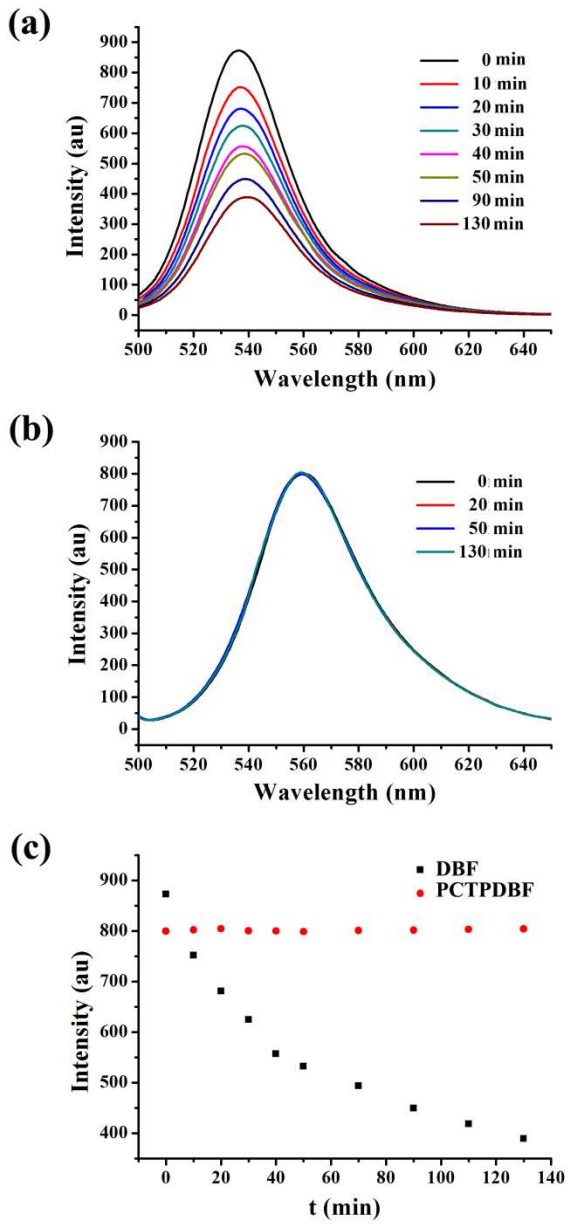

Fig. 6 Fluorescence spectra of (a) DBF (50 ug/mL) and (b) PCTPDBF NPs (300 ug/mL) in ethanol under 365 nm light (2 W) at different irradiation times, (c) plots of the fluorescence intensity of DBF and PCTPDBF NPs *vs.* different UV (365nm, 2 W) irradiation time.

The biocompatibility of PCTPDBF NPs was quantitatively assessed by MTT assays (Figure 8). The HeLa cells and H9C2 cells were chosen as the tumor and normal cell models, respectively. These two types of cells were incubated in PBS buffer containing PCTPDBF NPs of different concentrations for 24 and 48 h, separately. With the increase of nanoparticle concentration or elongation of the incubation time, the cell viability of HeLa cells and H9C2 cells was slightly reduced.

However, the cell viability was higher than 90% under all experimental conditions. Therefore, the PCTPDBF NPs are of biologically low cytotoxicity in MTT analysis in a wide concentration range from 0 to 100 μg/mL and exhibit potential for biomedical applications.

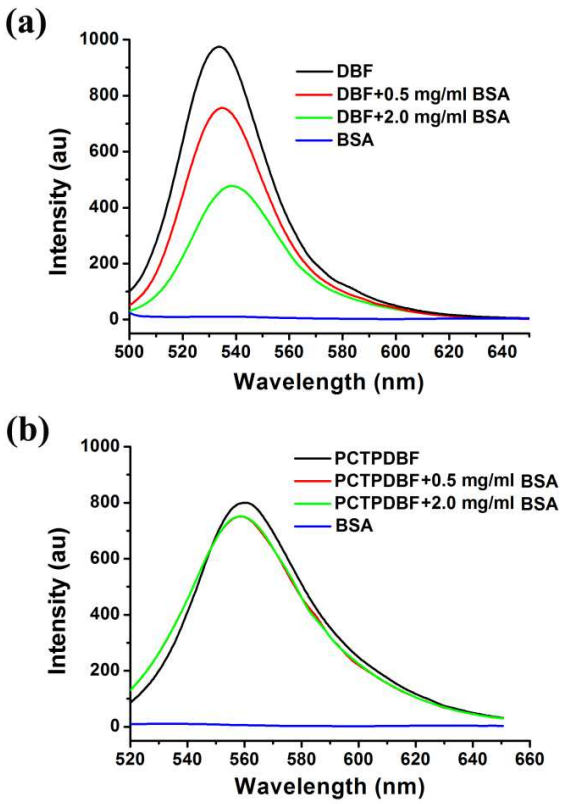

Fig. 7 Fluorescence spectra of (a) DBF (50 ug/mL) and (b) PCTPDBF (300 ug/mL) NPs mixed with BSA aqueous solution at different concentrations.

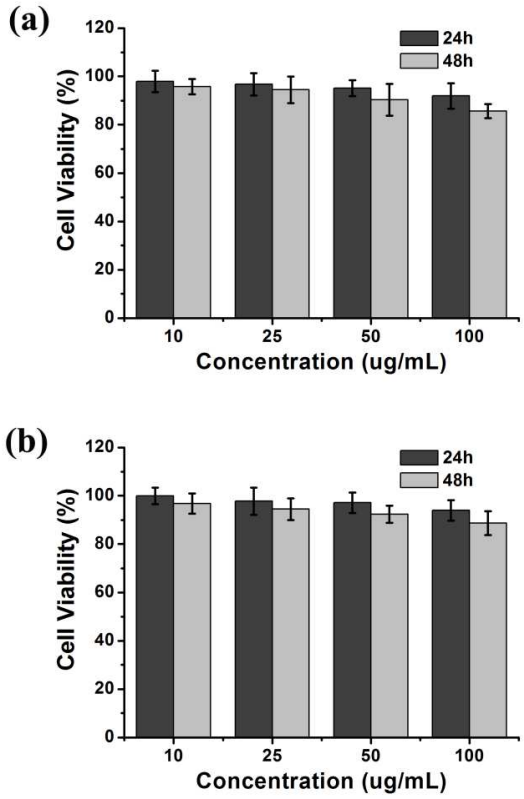

Fig. 8 Cell viability of (a) HeLa cells and (b) H9C2 cells after being cultured with PCTPDBF NPs at series of concentrations for 24 and 48 h.

Cite this: DOI: 10.1039/c0xx00000x

www.rsc.org/xxxxxx

Paper

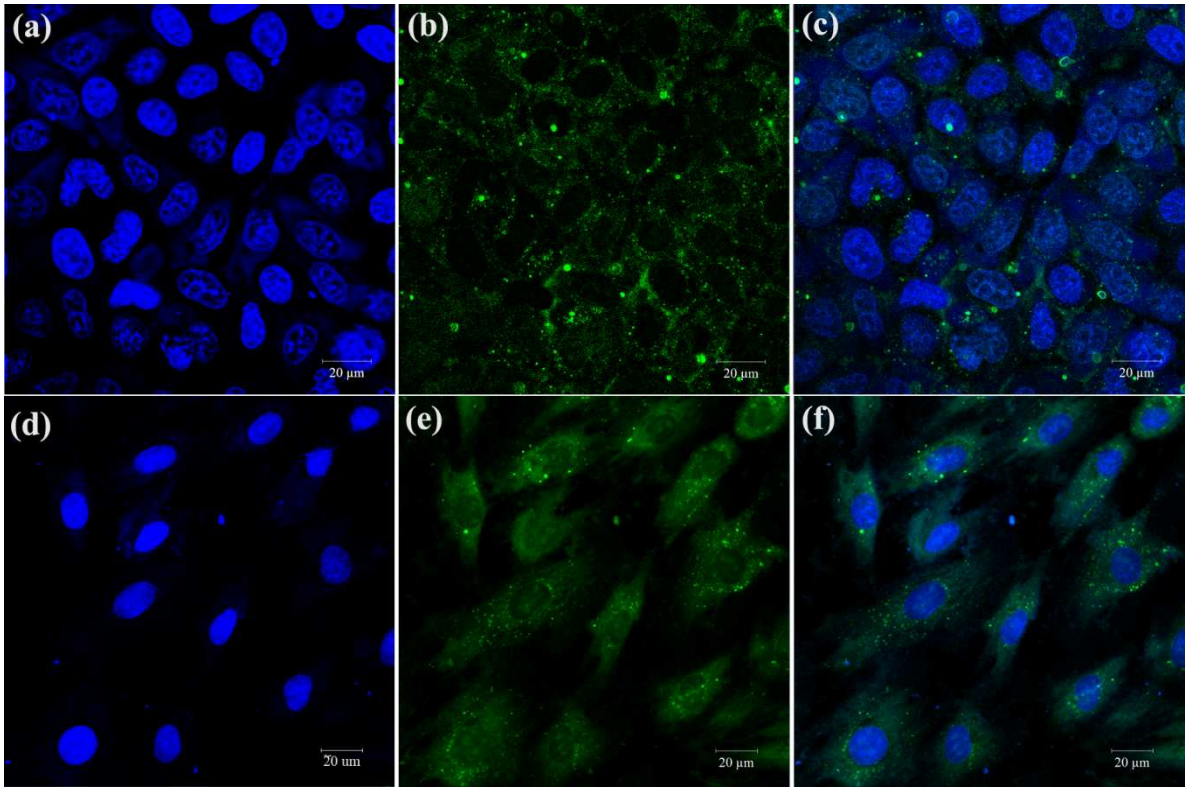

Fig. 9 Representative fluorescence images of (a–c) HeLa cells and (d–f) H9C2 cells incubated with 50 μg/mL PCTPDBF for 1h, washed with sterilized PBS, then fixed in paraformaldehyde (4 w%) for 10 min and stained in DAPI solution (0.1 μg/mL) for 20 min before being observed by a confocal laser scanning microscope under irradiation of (a, d) 360 nm, (b, e) 450 nm, (c, f) are the overlapping images

Based on their low toxicity, powerful fluorescence, and excellent resistance to photobleaching, PCTPDBF NPs were directly applied in cell imaging to demonstrate one of their promising applications (Figure 9). The HeLa and H9C2 cells were incubated with PCTPDBF NPs (50 μg/mL) for 1 h, washed with sterilized PBS, then fixed in paraformaldehyde (4 w%) for 10 min and stained in DAPI solution (0.1 μg/mL) for 20 min. Fluorescence images were recorded by confocal laser microscopy. After being stained by DAPI, the nuclei of HeLa cells exhibited bright blue fluorescence under irradiation with a 360 nm laser.[35,36] The PCTPDBF NPs emitted green fluorescence under irradiation by a 450 nm laser. HeLa cells and H9C2 cells incubated with PCTPDBF NPs exhibited bright blue and green images upon light irradiation of 360 and 450 nm, caused by the strong fluorescence emitted by DAPI and PCTPDBF, respectively (Figure 9a, b, d, and e). The PCTPDBF NPs should be mainly located in the cytoplasm because green fluorescence in the nucleus region was significantly weaker. When blue and green images were merged into one picture, whole cell images were perfectly obtained (Figure 9c and f).

4. Conclusions

Highly cross-linked and fluorescent polyphosphazene NPs were prepared by the facile one-pot polycondensation of HCCP and DBF. The morphology and size of the resulting PCTPDBF NPs can be well tuned by varying the solvent and reactant concentration. After being isolated and "fastened" in the cross-linked structures, the DBF moieties can effectively overcome the concentration-quenching effect. Therefore, PCTPDBF NPs emitted bright yellow fluorescence at any concentration. The PCTPDBF NPs entered the HeLa and H9C2 cells and were located in the cytoplasm. In addition, they also exhibited excellent biocompatibility and improved resistance to photobleaching and protein interference, thereby demonstrating potential to be used as an ideal fluorescent marker for cell imaging.

Acknowledgements

This work was supported by National Science Foundation for Distinguished Young Scholars (50925310), the National Science Foundation of China (21174087, 21474079), the Major Project of Chinese National Programs for Fundamental Research and

Development (973 Project: 2009CB930400), the Program for New Century Excellent Talents in University (NCET-13-0453), the China Postdoctoral Science Foundation (18420011, 2014T70909), the Fundamental Funds for the Central Universities (08142027, 08143101). The SEM was done at International Center for Dielectric Research (ICDR), Xi'an Jiaotong University; The authors thank Mr. Chuansheng Ma, Mr. Yanzhu Dai and Prof. Guang Yang for their help in using SEM.

Notes and references

[a] *School of Science; State Key Laboratory for Mechanical Behavior of Materials, Xi'an Jiaotong University, Xi'an, 710049, P.R. China. E-mail: menglingjie@mail.xjtu.edu.cn*
[b] *School of Chemistry and Chemical Technology; State Key Laboratory of Metal Matrix Composites, Shanghai Jiaotong University, Shanghai, 200240, P. R. China. Email: qhlu@sjtu.edu.cnA*
[c] *School of Life Science and Technology, Xi'an Jiaotong University, Xi'an, 710049, P.R. China.*

† Electronic Supplementary Information (ESI) available: TEM and SEM images of PCTPDBF synthesized in acetone and mixed solvent at various acetone/acetonitrile volume ratio, EDS spectrum of PCTPDBF, Fluorescence spectra of PCTPDBF nanoparticle ethanol solution prepared in acetone and acetonitrile, The photographs of PCTPDBF and BDF powder under nature light and 365nm UV-light. See DOI: 10.1039/b000000x/

1. T. Ozawa, H. Yoshimura and S. B. Kim, *Anal. Chem.*, 2013, **85**, 590-609.
2. A. Miyawaki, *Microscopy*, 2013, **62**, 63-68.
3. L. Yuan, W. Lin, K. Zheng, L. He and W. Huang, *Chem. Soc. Rev.*, 2013, **42**, 622-661.
4. S. J. Sahl and W. E. Moerner, *Curr. Opin. Struct. Biol.*, 2013, **23**, 778-787.
5. Y. Wang, J. Y. J. Shyy and S. Chien, in *Annu. Rev. Biomed. Eng.*, 2008, vol. 10, pp. 1-38.
6. E. Betzig, G. H. Patterson, R. Sougrat, O. W. Lindwasser, S. Olenych, J. S. Bonifacino, M. W. Davidson, J. Lippincott-Schwartz and H. F. Hess, *Science*, 2006, **313**, 1642-1645.
7. M. Chalfie, Y. Tu, G. Euskirchen, W. W. Ward and D. C. Prasher, *Science*, 1994, **263**, 802-805.
8. I. L. Medintz, H. T. Uyeda, E. R. Goldman and H. Mattoussi, *Nat. Mater.*, 2005, **4**, 435-446.
9. J. B. Blanco-Canosa, M. Wu, K. Susumu, E. Petryayeva, T. L. Jennings, P. E. Dawson, W. R. Algar and I. L. Medintz, *Coord. Chem. Rev.*, 2014, **263**, 101-137.
10. J. Zhou, Z. Liu and F. Li, *Chem. Soc. Rev.*, 2012, **41**, 1323-1349.
11. S. Gai, C. Li, P. Yang and J. Lin, *Chem. Rev.*, 2014, **114**, 2343-2389.
12. L. Changjun, Z. Peng, Z. Xinyun, T. Feng, L. Wenchen, Y. Jianhai, L. Yuan, W. Hongbo, W. Wei and L. Wenguang, *Biomaterials*, 2012, **33**, 3604-3613.
13. Y. P. Sun, B. Zhou, Y. Lin, W. Wang, K. A. S. Fernando, P. Pathak, M. J. Meziani, B. A. Harruff, X. Wang, H. F. Wang, P. J. G. Luo, H. Yang, M. E. Kose, B. L. Chen, L. M. Veca and S. Y. Xie, *J. Am. Chem. Soc.*, 2006, **128**, 7756-7757.
14. Z. Guo, S. Park, J. Yoon and I. Shin, *Chem. Soc. Rev.*, 2014, **43**, 16-29.
15. M. Montalti, L. Prodi, E. Rampazzo and N. Zaccheroni, *Chem. Soc. Rev.*, 2014, **43**, 4243-4268.
16. W. Xu-dong, R. J. Meier and O. S. Wolfbeis, *Adv. Funct. Mater.*, 2012, **22**, 4202-4207.
17. D. M. Shcherbakova, O. M. Subach and V. V. Verkhusha, *Angew. Chem. Int. Ed.*, 2012, **51**, 10724-10738.
18. U. Resch-Genger, M. Grabolle, S. Cavaliere-Jaricot, R. Nitschke and T. Nann, *Nat. Methods*, 2008, **5**, 763-775.
19. P. Babula, V. Adam, R. Opatrilova, J. Zehnalek, L. Havel and R. Kizek, *Environ. Chem. Lett.*, 2008, **6**, 189-213.
20. P. Miao, K. Han, Y. Tang, B. Wang, T. Lin and W. Cheng, *Nanoscale*, 2015, **7**, 1586-1595.
21. S. Y. Lim, W. Shen and Z. Gao, *Chem. Soc. Rev.*, 2015, **44**, 362-381.
22. Y. Hong, J. W. Y. Lam and B. Z. Tang, *Chem. Soc. Rev.*, 2011, **40**, 5361-5388.
23. C. Eggeling, J. Widengren, L. Brand, J. Schaffer, S. Felekyan and C. A. M. Seidel, *J. Phys. Chem. A*, 2006, **110**, 2979-2995.
24. M. J. Ruedas-Rama, J. D. Walters, A. Orte and E. A. H. Hall, *Anal. Chim. Acta*, 2012, **751**, 1-23.
25. X. J. Zhao, R. P. Bagwe and W. H. Tan, *Adv. Mater.*, 2004, **16**, 173-176.
26. J. D. Luo, Z. L. Xie, J. W. Y. Lam, L. Cheng, H. Y. Chen, C. F. Qiu, H. S. Kwok, X. W. Zhan, Y. Q. Liu, D. B. Zhu and B. Z. Tang, *Chem. Commun.*, 2001, 1740-1741.
27. Y. Hu, L. Meng and Q. Lu, *Langmuir*, 2014, **30**, 4458-4464.
28. J. Zhou, L. Meng, X. Feng, X. Zhang and Q. Lu, *Angew. Chem. Int. Ed.*,2010, **49**, 8476-8479.
29. J. Zhou, L. Meng, Q. Lu, J. Fu and X. Huang, *Chem. Commun.*, 2009, 6370-6372.
30. L. Meng, X. Zhang, Q. Lu, Z. Fei and P. J. Dyson, *Biomaterials*, 2012, **33**, 1689-1698.
31. X. Zhang, L. Meng, Q. Lu, Z. Fei and P. J. Dyson, *Biomaterials*, 2009, **30**, 6041-6047.
32. E. C. C. Goh and H. D. H. Stover, *Macromolecules*, 2002, **35**, 9983-9989.
33. Y. Hu, L. Meng, L. Niu and Q. Lu, *Langmuir*, 2013, **29**, 9156-9163.
34. J. Zhou, L. Meng and Q. Lu, *J. Mater. Chem.*, 2010, **20**, 5493-5498.
35. H. R. Allcock, T. X. Neenan and B. Boso, *Inorg. Chem.*, 1985, **24**, 2656-2662.
36. H. Ow, D. R. Larson, M. Srivastava, B. A. Baird, W. W. Webb and U. Wiesner, *Nano Lett.*, 2005, **5**, 113-117.
37. M. J. Saunders, E. Block, A. Sorkin, A. S. Waggoner and M. P. Bruchez, *Bioconj. Chem.*, 2014, **25**, 1556-1564.
38. Z. Ji, X. Liang, Y. Sun and J. Fan, *Asian J. Chem.*, 2014, **26**, 521-526.
39. O. K. Abou-Zied and S. A. J. Sulaiman, *Dyes and Pigments*, 2014, **110**, 89-96.

Table of contents entry

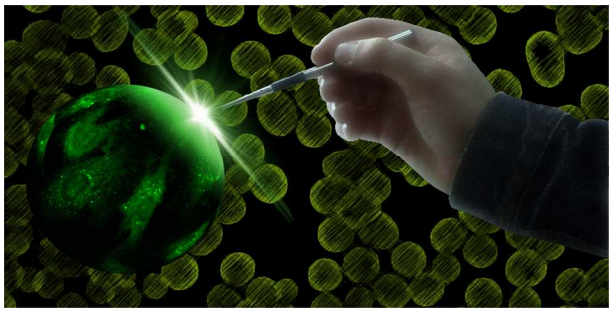

Highly cross-linked and fluorescent polyphosphazene nanoparticles with excellent biocompatibility and improved resistance to photobleaching and protein interference were prepared for cell imaging.